Tropical Cyclone Outflow-Layer Structure and Balanced Response to Eddy Forcings

SARAH D. DITCHEK, JOHN MOLINARI, AND DAVID VOLLARO

Department of Atmospheric and Environmental Sciences, University at Albany, State University of New York, Albany, New York

(Manuscript received 15 April 2016, in final form 28 July 2016)

ABSTRACT

The ERA-Interim is used to generate azimuthally averaged composites of Atlantic basin tropical cyclones from 1979 to 2014. Both the mean state and the eddy forcing terms exhibited similar radial–vertical structure for all storm intensities, varying only in magnitude. Thus, only major hurricanes are described in detail. Radial inflow and outflow extended beyond the 2000-km radius. Warm anomalies reached 2000 km in the outflow layer. Composite eddy momentum fluxes within the outflow layer were 2.5 times larger than mean momentum fluxes, highlighting the importance of outflow–environment interactions. A balanced vortex equation was applied to understand the role of eddy heat and momentum fluxes. Dominant terms were the lateral eddy heat flux convergence, lateral eddy momentum flux, and eddy Coriolis torque. Each acted to enhance the secondary circulation. The eddy momentum flux terms produced about twice the response of heat flux terms. The circulation created by the eddy Coriolis torque arises from a vertical gradient of mean storm-relative meridional wind in the upper troposphere at outer radii. It is produced by background inertial stability variations that allow stronger outflow on the equatorward side. Overall, the fluxes drive a strengthened secondary circulation that extends to outer radii. Balanced vertical motion is strongest in the upper troposphere in the storm core. A method is proposed for evaluating the role of environmental interaction on tropical cyclone intensity change.

1. Introduction

The tropical cyclone outflow layer has sometimes been treated as a passive recipient of air from the eyewall. In the theory of Emanuel (1986), outflow-layer entropy and angular momentum, except at very large radii, were set by their values in the storm core in the boundary layer. Recently, however, Emanuel and Rotunno (2011) offered an alternative closure that allowed variations in potential temperature in the outflow. Their closure requires a critical Richardson number be met, and the structure of the tropical cyclone in the core was coupled to this assumption, making the outflow layer a more active contributor to the storm.

Anthes (1974) noted that outflow in tropical cyclones plays two primary roles. First, it removes anticyclonic angular momentum from the storm at larger radii. Anthes (1974) argued that such lateral fluxes across an outer boundary were the only source of angular momentum in the storm to offset that lost to friction. In addition, outflow removes high-entropy air from the storm core. This removal appears as a source term in the available potential energy budget (Anthes 1974). Without such entropy fluxes, the outflow air would subside and warm, and thus reduce the radial temperature gradient and over time weaken the storm.

Tropical cyclone outflow layers are asymmetric, typically breaking down into one or two anticyclonic outflow jets. As a result, lateral fluxes of heat and momentum are carried both by the azimuthal mean flow and by eddies. Pfeffer and Challa (1981) forced a symmetric model with composite observed lateral eddy fluxes of angular momentum from McBride (1981). Eddy momentum fluxes peaked at large radii within the narrow outflow layer. The model was run with a composite developing storm and then with a composite nondeveloping storm, each with its own composite lateral eddy momentum flux. Pfeffer and Challa (1981) found that the composite developing storm rapidly intensified into a model hurricane. The composite nondeveloping storm with its diffuse eddy fluxes did not intensify. Most importantly, removing the eddy momentum fluxes from the developing storm prevented it

Corresponding author e-mail: Sarah D. Ditchek, sarahditchek@gmail.com

DOI: 10.1175/JAS-D-16-0117.1

from intensifying, even after 20 days. The authors hypothesized that a deep balanced response to these fluxes created enhanced radial circulation in the storm that contributed to its development. In this framework, outflow eddies provide meaningful forcing of tropical cyclone intensification. One limitation of the Pfeffer and Challa (1981) paper was that no other eddy terms were considered.

Molinari and Vollaro (1989) used observations to study eddy forcings in Hurricane Elena (1985) during a period when an upper-tropospheric, midlatitude trough moved toward the storm center. A manually derived set of 200-hPa cloud motion vector observations supplemented the rawinsonde network. As the upper-tropospheric trough approached the storm, large eddy momentum fluxes shifted inward with time, accompanied by enhanced outflow, consistent with the balanced arguments. Rapid intensification resulted as the induced outflow reached the storm core.

Molinari and Vollaro (1990), using operational analyses from ECMWF, found fluxes to be remarkably similar to those from observations. This allowed a full global model evaluation of all eddy heat and momentum flux terms and a formal balanced model response to these fluxes. The results supported the role of eddy momentum forcing in driving upward motion in the storm core just prior to rapid intensification. Lateral eddy heat fluxes contributed to enhanced radial circulation as well, but their effect was secondary. Molinari and Vollaro (1990) thus showed that global model analyses, despite being unable to see details in the tropical cyclone core, provided a powerful tool for evaluating the roles of outflow-layer eddies. However, they considered only a single case study, specifically a trough interaction case. Additionally, 30 years ago resolution of the ECMWF analyses was coarse—the spatial resolution was 2.5° and only seven pressure levels were used.

DeMaria and Kaplan (1994) found that eddy momentum flux convergence at 200 hPa provided a useful predictor in a statistical tropical cyclone intensity forecast. This eddy flux term by itself was insufficient: vertical wind shear, deviation of the storm from its potential intensity, and prior intensity change also had to be included. The intent in this paper is not to design such a prediction scheme using eddy terms. Rather, it is to extend the results of Molinari and Vollaro (1990) to a large number of cases. We evaluate the impact of eddy fluxes of heat and momentum, both together and separately, on the secondary circulation of tropical cyclones, and provide physical interpretations for each forcing term. The ERA-Interim (Dee et al. 2011) is used to generate Atlantic basin tropical cyclone composite structure and eddy forcing over a 36-yr period (1979–2014). The goal is to provide a formal integrated measure of environmental interactions in tropical cyclones.

TABLE 1. The original and remaining number of tropical cyclone center times after applying four filters to the data.

Label	Original	Subset
Tropical depression	3837	2922
Tropical storm	4829	3820
All hurricanes	3367	2765
Minor (categories 1 and 2) hurricanes	2633	2025
Major (categories 3–5) hurricanes	813	740

2. Data

a. Tropical cyclone data

Four-times-daily Atlantic basin tropical cyclone location and intensity were obtained from the second-generation NHC ''best track'' hurricane database (HURDAT2; Landsea and Franklin 2013). Because of the subjective nature of HURDAT2, uncertainties in position and intensity are present. A detailed description of uncertainties is provided in Torn and Snyder (2012) and in Landsea and Franklin (2013).

A subset of the HURDAT2 data was extracted by implementing four filters to 1) keep storms of tropical depression or greater strength, 2) remove times after the storm center passed 40°N regardless of whether the storm center eventually moved south of 40°N in order to reduce mid- and high-latitude influences, 3) remove extratropical or subtropical storms, and 4) remove times after a storm made landfall for greater than 6 h. Tropical cyclone center times were stratified by intensity into four groupings: tropical depressions, tropical storms, and Saffir–Simpson hurricane wind scale minor (categories 1–2) and major (categories 3–5) hurricanes (Simpson 1974). Table 1 lists the original and remaining sample sizes of tropical cyclone center times that fit these criteria.

b. Numerical model analyses

Zonal and meridional components of the wind, potential temperature, and vertical velocity were retrieved from the 6-hourly ERA-Interim data. The ERA-Interim is available on 37 pressure levels with a horizontal resolution of 0.7° × 0.7°. Although the ERA-Interim input data have evolved during our period of interest, the analyses have major benefits when comparing storms over many years: identical model physics, model resolution, and initialization procedures. These analyses contain substantial input from all real-time observations. The gridded analyses thus represent a hybrid

numerical model plus observed data depiction of the atmosphere.

The global analyses represent every radius and azimuth in every storm of all intensities over the 36-yr period. This is a major advantage not present in any directly measured data such as those studies that have utilized rawinsondes (e.g., Frank 1977a; McBride 1981). Rawinsondes have the disadvantages of uneven distribution in space and time and from storm to storm, rarely sampling the storm core, and insufficient data at outer radii (beyond r = 800–1000 km) where environmental forcing is important.

Two primary disadvantages exist in the global analyses (Schenkel and Hart 2012): 1) the center position in the analysis often differs somewhat from that in nature and 2) they cannot resolve the storm core, and thus they underestimate the intensity of the storms.

The influence of the incorrect center positions produces one artifact at small radii in the eddy momentum flux convergence forcing field. To remove that problem, the eddy forcing was linearly interpolated from the 400-km radius to zero at the center. The first part of appendix A shows that, with one small exception, the balanced solutions are virtually unaffected by this interpolation. As a result, this deficiency of the global analyses has only a small impact on the overall solutions.

The second issue, the underestimate of intensity, could in principle produce unrealistic responses because the inertial stability in the storm core will be too small. The second part of appendix A addresses this issue. It is shown that the balanced response to major hurricane eddy forcing hardly changes at all when a tropical depression mean state is substituted for the major hurricane base state. This insensitivity arises from two factors: 1) the storm core represents a small area and the inverse Laplacian operator in the balanced solution tends to smooth out the response to such regions, and 2) as will be seen later, the eddy forcing is largest at middle and outer radii.

3. Composites: Methods

Data were bilinearly interpolated to cylindrical grids centered on each individual tropical cyclone center radially every 100 km (from 100 to 2000 km outside the storm core) and vertically every 25 hPa (from 1000 to 50 hPa). Zonal and meridional winds were transformed into radial v_r and tangential v_λ velocity. Radial–vertical cross sections of azimuthally averaged variables will be shown.

Regions where major hurricanes differed significantly from tropical depressions at the 99% confidence were determined through bootstrap testing with 1000 iterations. Significant differences will be shown by stippling in figures. All mentions of significant differences in the text of this paper will refer to this bootstrap method.

4. Composites: Results

a. Divergence and relative vorticity

Azimuthally averaged horizontal divergence (Figs. 1a–d) and relative vorticity (Figs. 1e–h) are given by

$$\overline{D} = \frac{\partial(\overline{v}_r)}{\partial r} + \frac{\overline{v}_r}{r} \quad \text{and} \tag{1}$$

$$\overline{\zeta} = \frac{\partial(\overline{v}_\lambda)}{\partial r} + \frac{\overline{v}_\lambda}{r}, \tag{2}$$

where

$$\overline{(\,)} = \frac{1}{2\pi}\int_0^{2\pi} (\,)\, d\lambda\,. \tag{3}$$

Divergence (Figs. 1a–d) peaks at 175 hPa and at the 100-km radius regardless of storm intensity. Convergence is located in the inflow layer with largest values at 950 hPa and at the 100-km radius, again regardless of intensity. With an increase in intensity, there is both stronger divergence aloft and stronger convergence below.

Within the entire outflow layer and throughout the troposphere from 500 km outward, there is anticyclonic relative vorticity (Figs. 1e–h) that increases in magnitude with intensity. With increasing intensity the maximum anticyclone remains at 175 hPa and at the 400-km radius. At inner radii, cyclonic relative vorticity dominates. As intensity increases, the cyclone extends over a deeper layer, and the intense upper-tropospheric updrafts lift the tropopause in the core.

As seen in the divergence and relative vorticity composite fields (Fig. 1), structural similarities among intensities are present. Differences among intensities primarily manifest in the magnitude of the variable. This is true for eddy heat and momentum fluxes as well (appendix B). Thus, from this point forward, only the composite for major hurricanes will be discussed.

b. Wind fields

The radial wind composite is shown in Fig. 2a. The primary outflow exists from 100 to 300 hPa in the upper troposphere at inner radii and peaks at 175 hPa at the 600-km radius. At outer radii, the outflow narrows to a 100-hPa layer and extends beyond 2000 km. Near the storm center, inflow is maximized in the boundary layer at around 200 km from the storm center and is present from

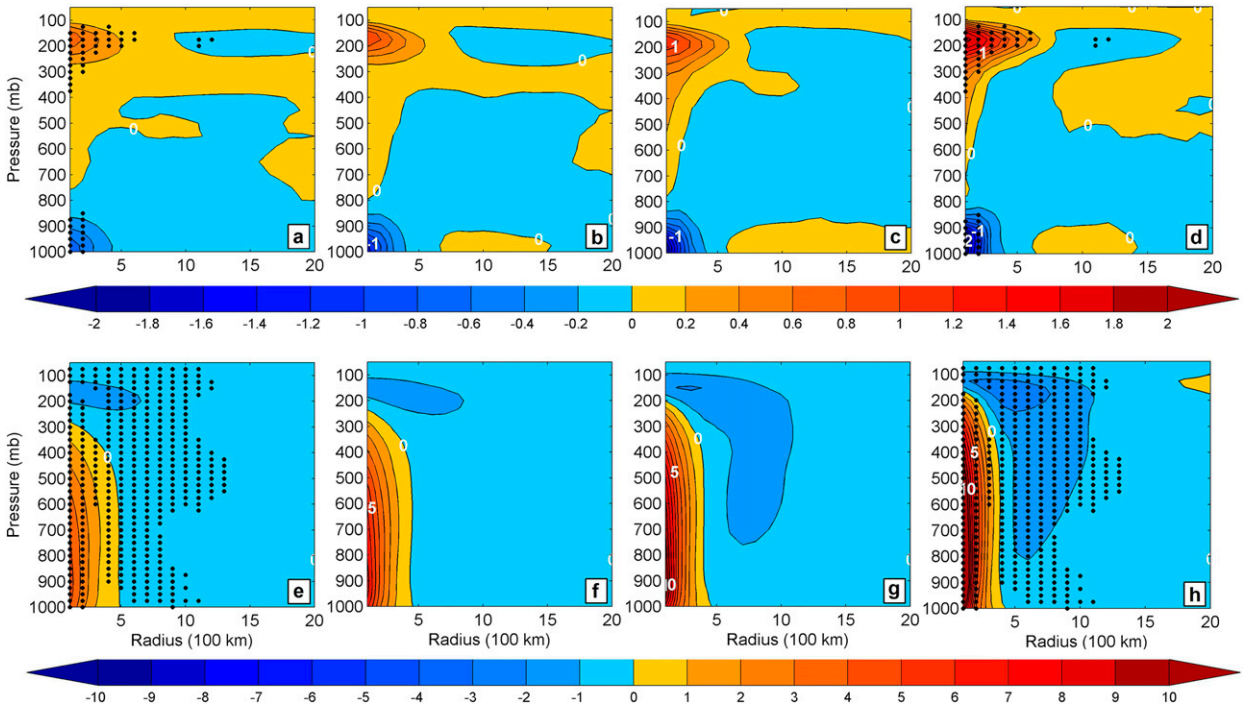

FIG. 1. Composites of (a)–(d) divergence (contour interval: $0.2 \times 10^{-5}\,s^{-1}$) and (e)–(h) relative vorticity (contour interval: $1 \times 10^{-5}\,s^{-1}$) for (a),(e) tropical depressions; (b),(f) tropical storms; (c),(g) minor hurricanes; and (d),(h) major hurricanes. The sample size used to generate the composites is 2922, 3820, 2765, and 740, respectively. Stippling (dots) indicates locations of significant differences at the 99% confidence level between the weakest (tropical depressions) and strongest (major hurricanes) intensity of the same variable as calculated by a bootstrap test.

the storm center to beyond 2000 km outside the storm center. Inflow extends into the middle troposphere outside $r = 400$ km. Significant differences in radial velocity between tropical depressions and major hurricanes exist almost wholly in the narrow inflow and outflow layers.

The second panel of Fig. 2 is the tangential wind composite. Aloft, the outflow layer is associated with anticyclonic flow from the inner radii where it is concentrated in the upper troposphere to outer radii where it reaches the surface. The maximum anticyclonic flow is located at 150 hPa at the 1200-km radius. The cyclonic circulation at the surface extends from inner radii to the 1400-km radius and is present from the surface to 150 hPa at inner radii. The maximum in the cyclonic flow is at 900 hPa at inner radii.

c. Potential temperature

The anomalous potential temperature composite field (Fig. 3) is calculated relative to the mean moist tropical sounding from Dunion (2011). A warm anomaly is present from 150 to 900 hPa at inner to middle radii and peaks in the upper troposphere at 250 hPa at inner radii. Negative values immediately above this warm core indicate that the tropopause is higher and colder than the typical moist tropical environment. Previous studies have shown that a tropical cyclone is a warm-core system in the inner-core region, from the storm center to about the 150-km radius (e.g., Stern and Nolan 2012). Here, the potential temperature anomaly field is presented on a much larger scale, with warm anomalies reaching 2000 km in the outflow layer.

d. Momentum fluxes

Figure 4 shows radial–vertical cross sections of mean (Fig. 4a) and eddy momentum (Fig. 4b) fluxes (Molinari and Vollaro 1989) given by

$$\left(\frac{\partial \overline{M}}{\partial t}\right)_{\text{meanflux}} = -\frac{2\pi r^2}{g}\int_p \overline{v}_r \overline{v}_\lambda \, dp \quad \text{and} \tag{4}$$

$$\left(\frac{\partial \overline{M}}{\partial t}\right)_{\text{eddyflux}} = -\frac{2\pi r^2}{g}\int_p \overline{v_r' v_\lambda'} \, dp\,, \tag{5}$$

where primes indicate deviations from the azimuthal mean and $dp = 25$ hPa. Values are calculated within each layer from 1000 to 50 hPa. Positive values in Fig. 4 indicate a source of relative angular momentum to the volume produced by fluxes across the given radius. Hereafter, mentions of momentum will denote relative angular momentum unless otherwise specified.

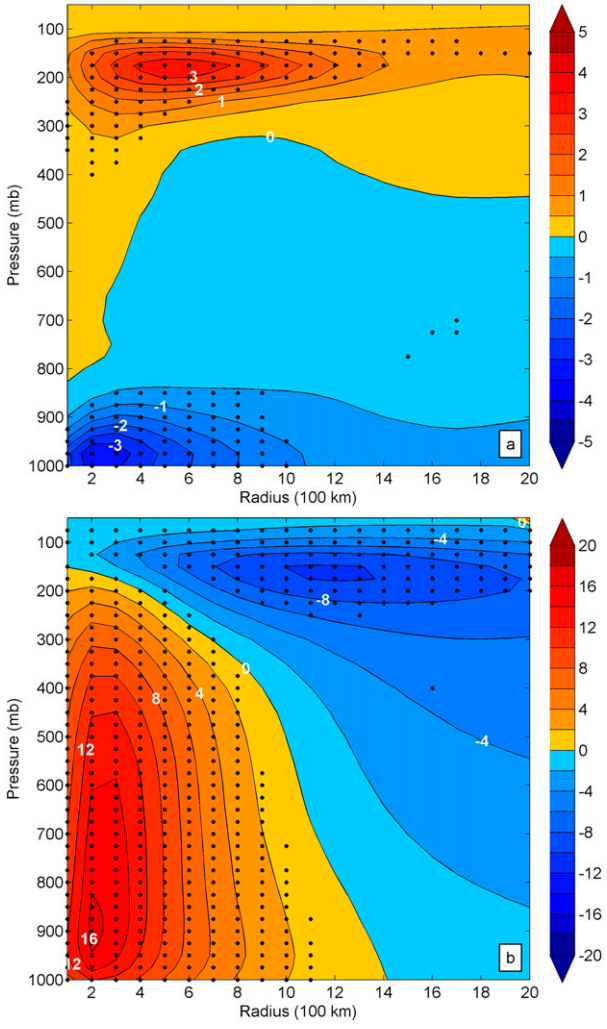

FIG. 2. Composites of (a) radial (contour interval: 0.5 m s^{-1}) and (b) tangential (contour interval: 2 m s^{-1}) wind for major hurricanes. The sample size used to generate the composites is 740. Stippling (dots) indicates regions of significant differences between tropical depressions and major hurricanes as calculated by a bootstrap test.

The mean flux (Fig. 4a) is largest in the upper troposphere near 200 hPa and at the 1200-km radius. It is consistent with Fig. 2: mean outflow removes negative angular momentum. Thus, the outflow layer acts as a momentum source as there is an inward flux of momentum. The mean momentum flux is relatively small in other parts of the storm. The term is positive in the lower troposphere, where mean inflow carries mean cyclonic momentum toward the center, but the magnitude is much smaller than the outflow-layer source.

Like the mean flux, the eddy term (Fig. 4b) contains a narrow outflow-layer maximum with large vertical gradients above and below, consistent with the distributions shown by Pfeffer and Challa (1981) and Fig. 5 in Molinari and Vollaro (1990). Eddy fluxes are small

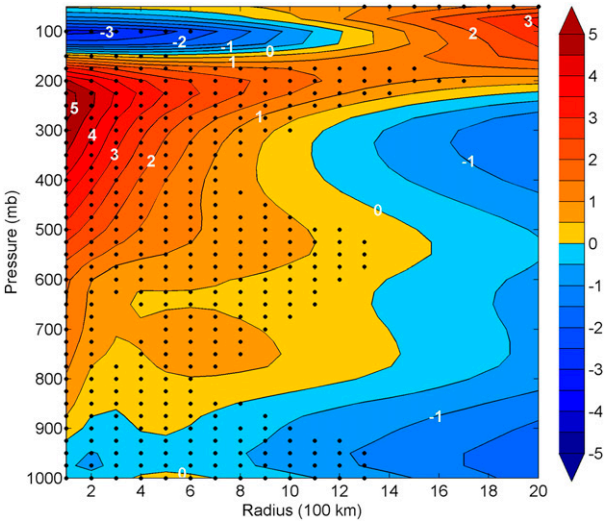

FIG. 3. As in Fig. 2, but for the potential temperature anomaly (contour interval: 1 K) in reference to the Dunion (2011) moist tropical sounding. A 1–2–1 smoother in the vertical was applied for aesthetic purposes.

elsewhere. The eddy momentum fluxes arise within anticyclonic outflow jets, which act as a source by removing negative eddy momentum from the volume. Interactions with upper-tropospheric troughs also create an eddy momentum source by carrying positive eddy momentum inward northwest of the tropical cyclone [see Fig. 9 in Molinari and Vollaro (1989)]. The strongest eddy momentum flux lies in the outflow layer at about the 1600-km radius. Overall, the eddy fluxes exceed the mean fluxes by a factor of 2.5 averaged over the region from $r = 600$ to 2000 km and from $p = 150$ to 250 hPa. The response to these eddy fluxes will be addressed in section 7.

5. Balanced model: Methods

Equations

A streamfunction ψ is used to visualize the effects of the eddy-induced radial–vertical circulation. It is given by

$$\overline{v}_r = \frac{1}{r}\frac{\partial \psi}{\partial p} \quad \text{and} \tag{6}$$

$$\overline{\omega} = -\frac{1}{r}\frac{\partial \psi}{\partial r}. \tag{7}$$

The full balanced vortex equation is given by

$$A\psi_{pp} + 2B\psi_{rp} + C\psi_{rr} - \frac{4B}{r}\psi_p - \left(\frac{1-\kappa}{p}B + \frac{C}{r}\right)\psi_r = r\frac{\partial}{\partial p}\left[\left(\frac{2\overline{v}_\lambda}{r} + f\right)\left(\frac{\partial \overline{v}_\lambda}{\partial t}\right)_{\text{eddy}}\right] + \frac{r\pi R}{p}\frac{\partial}{\partial r}\left(\frac{\partial \overline{\theta}}{\partial t}\right)_{\text{eddy}}, \tag{8}$$

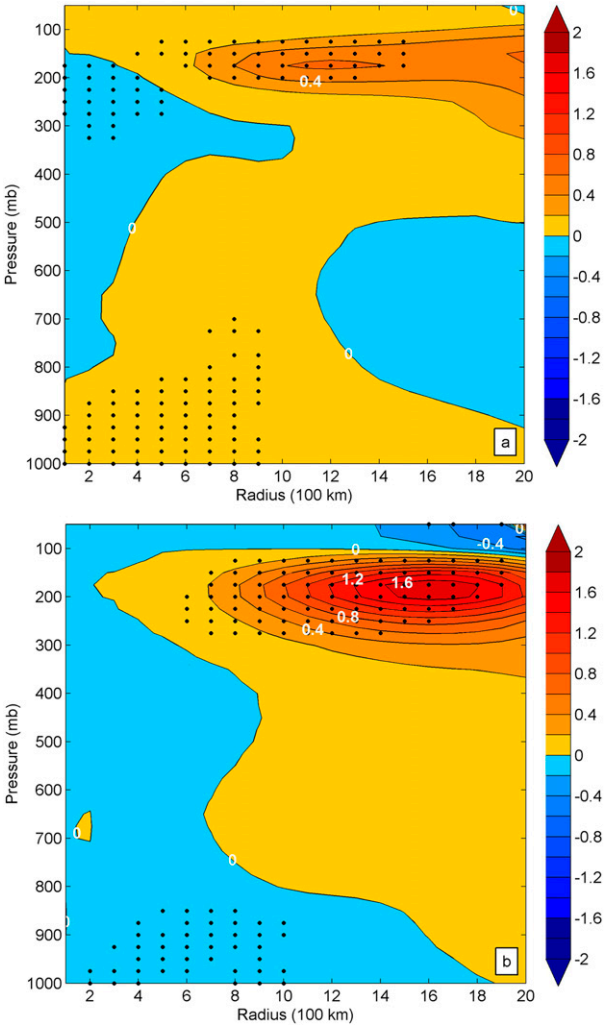

FIG. 4. As in Fig. 2, but for (a) mean momentum flux [Eq. (4)] and (b) eddy momentum flux [Eq. (5)] for major hurricanes. Both composites' contour intervals are $0.2 \times 10^{16}\,\mathrm{kg\,m^2\,s^{-2}}$.

where the subscripts of ψ represent partial derivatives and

$$\pi = \left(\frac{p}{p_o}\right)^{R/c_p}. \tag{9}$$

The left-hand side of the equation contains three coefficients:

$$A = \left(f + \frac{2\overline{v}_\lambda}{r}\right)\left(f + \frac{\partial \overline{v}_\lambda}{\partial r} + \frac{\overline{v}_\lambda}{r}\right), \tag{10}$$

$$B = -\left(f + \frac{2\overline{v}_\lambda}{r}\right)\left(\frac{\partial \overline{v}_\lambda}{\partial p}\right), \quad \text{and} \tag{11}$$

$$C = -\frac{R\pi}{p}\frac{\partial \overline{\theta}}{\partial p}, \tag{12}$$

where A is the inertial stability, B is the baroclinicity, and C is the static stability.

The right-hand side consists of the eddy tangential velocity source and the eddy heat source. They are given by

$$\left(\frac{\partial \overline{\theta}}{\partial t}\right)_{\text{eddy}} = -\frac{1}{r}\frac{\partial(r\overline{\theta' v_r'})}{\partial r} - \frac{\partial(\overline{\theta'\omega'})}{\partial p} \quad \text{and} \tag{13}$$

$$\left(\frac{\partial \overline{v}_\lambda}{\partial t}\right)_{\text{eddy}} = -\frac{1}{r^2}\frac{\partial(r^2\overline{v_r' v_\lambda'})}{\partial r} - \frac{\partial(\overline{\omega' v_\lambda'})}{\partial p} - \overline{f' v_r'}, \tag{14}$$

where primes indicate deviations from the azimuthal mean. The eddy heat source is the summation of 1) the horizontal eddy temperature flux convergence and 2) the vertical eddy temperature flux convergence. The eddy tangential velocity source is the summation of 1) the horizontal eddy flux convergence of tangential wind, 2) the vertical eddy flux convergence of tangential wind, and 3) the eddy Coriolis torque.

Of interest is to determine the impact of large-scale eddy heat and momentum forcings on the secondary circulation of tropical cyclones. Diabatic effects were not included, consistent with work done in Molinari and Vollaro (1990). Therefore, the solutions shown in this work represent the adiabatic responses of tropical cyclones to heat and momentum fluxes. Diabatic terms not included will couple with these adiabatic forcings. Since the balanced vortex equation itself is a linear equation, the response to the individual heat and momentum forcings can be shown separately. The solution to Eq. (8) is carried out following Molinari and Vollaro (1990).

Forcing terms are remarkably similar structurally regardless of intensity (see appendix B). Thus, only the responses for major hurricanes will be discussed.

6. Balanced model: Left-hand-side coefficients

Following Holland and Merrill (1984), inertial stability [Eq. (10)] was normalized by f_0^2, where f_0 is the mean latitude of all tropical depression and major hurricane occurrences.[1] To better display low inertial stability, the log (base 2) was taken. The zero line corresponds to the ratio of inertial stability to f_0^2 being equal to 1, indicating that the inertial stability of major hurricanes is equal to the background environmental inertial stability. The weakest inertial stability is located in the outflow layer (Fig. 5a), indicating that the outflow layer can more easily interact with the environment (Rappin et al. 2011). It is this

[1] The average latitude of tropical depressions and major hurricanes was calculated since statistical significance testing is performed between these two categories.

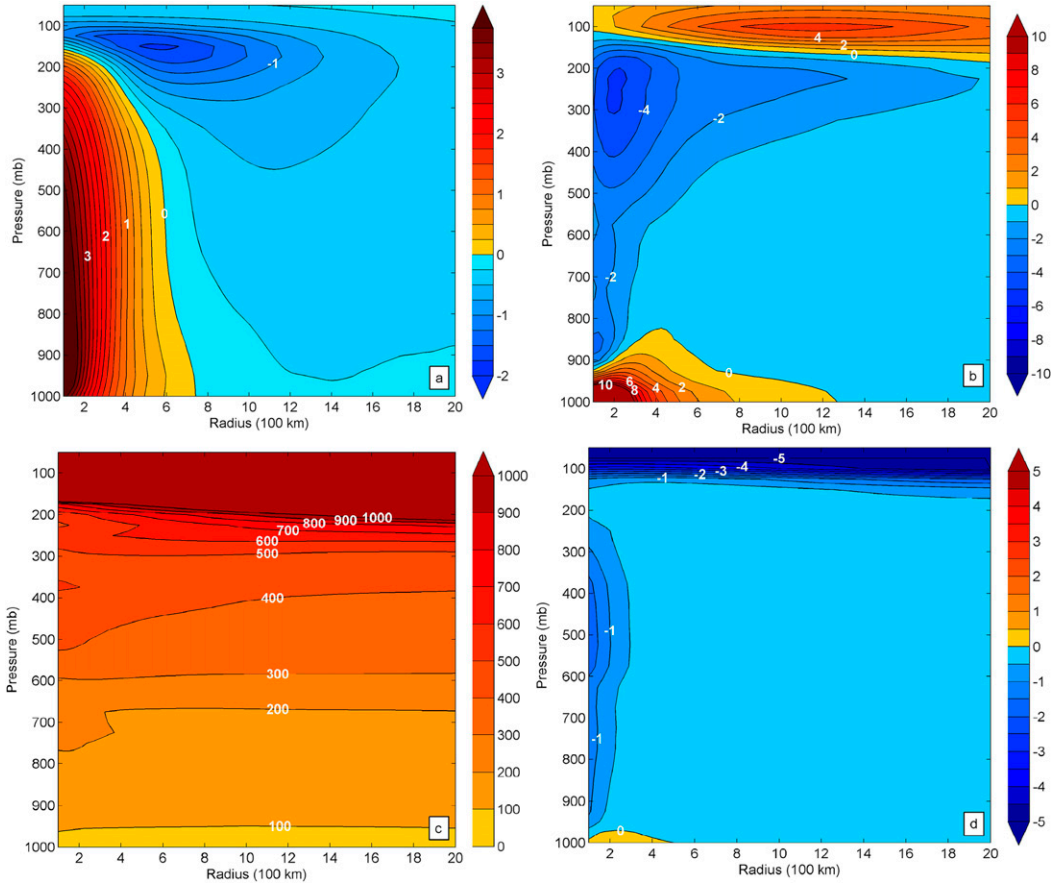

FIG. 5. Depictions of (a) the log (base 2) of the ratio of inertial stability to f^2 (contour interval: 0.25), (b) baroclinicity (contour interval: $1 \times 10^{-8}\,\mathrm{m^2\,kg^{-1}}$), (c) static stability (contour interval: $100 \times 10^{-8}\,\mathrm{m^4\,s^2\,kg^{-2}}$), and (d) $B^2 - AC$ (contour interval: $0.5 \times 10^{-13}\,\mathrm{m^4\,kg^{-4}}$).

environmental interaction that is a source of eddy transport. This effect is seen in Fig. 4b, where there is a large inward flux of momentum in the outflow layer by eddies. The minimum in inertial stability occurs in the outflow layer at 600 km, coinciding with the maximum radial outflow (Fig. 2a). Weak inertial stability exists throughout the troposphere at outer radii as well. As expected, the core of major hurricanes is highly inertially stable.

The second panel of Fig. 5 is the baroclinicity [Eq. (11)]. Positive values indicate tangential velocity increasing upward. The outflow layer has a tangential wind minimum at 150 hPa at the 1200-km radius (Fig. 2b). It is at this pressure level that the baroclinicity reverses in the upper troposphere from negative to positive. A core assumption of the balanced vortex equations is gradient wind balance. This balance is not met in the boundary layer of tropical cyclones. As a result, the large baroclinicity term near the surface reflects the upward increase of tangential velocity in the friction layer rather than the presence of a strong radial temperature gradient.

The static stability is shown in the third panel of Fig. 5 [Eq. (12)]. Static stability is smallest at the surface and increases upward throughout the troposphere. Stability jumps to large values in the stratosphere.

Equation (8) is elliptic if $B^2 - AC$, shown in the last panel of Fig. 5, is less than 0. This condition is met at all but 0.7% of grid points. Those grid points are located at 975–1000 hPa at inner radii owing to the breakdown of the balanced vortex assumptions in the boundary layer–gradient wind balance is not met. In that region, the large, positive B^2 term dominates the AC term, hence creating $B^2 - AC > 0$. Despite the ellipticity condition not being met in some locations, the balanced vortex solution was still able to converge, indicating that imbalances are not large.

7. Balanced model: Responses to eddy forcings

The balanced vortex equation is applied on composited fields rather than averaging the balanced response

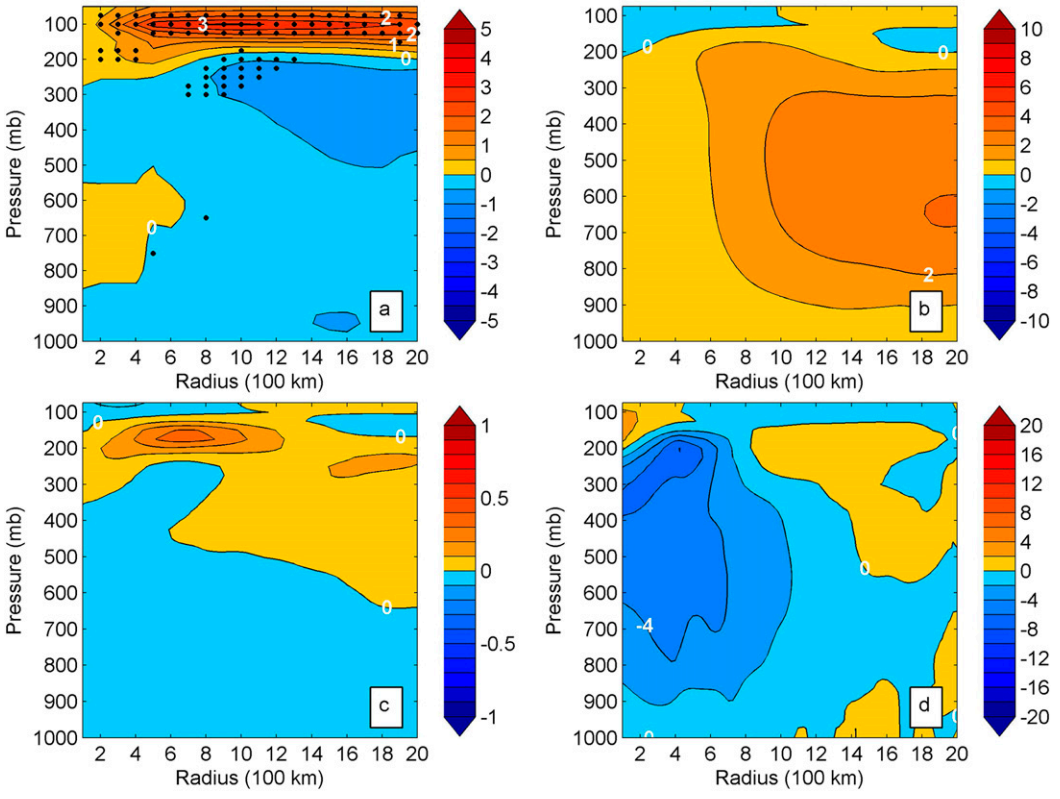

FIG. 6. The lateral eddy heat flux convergence [Eq. (13), term 1] (a) composite (contour interval: 0.5 K day^{-1}), (b) balanced vortex response (contour interval: 1 × 10^9 Pa m^2 s^{-1}), (c) radial wind response (contour interval: 0.1 m s^{-1}), and (d) vertical velocity response (2 hPa day^{-1}). Stippling (dots) in (a) indicates regions of significant differences between tropical depressions and major hurricanes as calculated by a bootstrap test.

of each individual storm time in order to determine the response of a typical vortex to eddy heat and momentum sources. A similar approach was performed by Holland and Merrill (1984).

The response of the vortex to the three dominant eddy heat and momentum source terms in Eqs. (13) and (14) is shown in Figs. 6–8. Figures 6a, 7a, and 8a will depict the composite forcing with overlying stippling interpreted as in earlier figures. Figures 6b, 7b, and 8b will depict the streamfunction response. In interpreting the streamfunction, it is the gradients of the streamlines that are important rather than their relative magnitudes. Thus, negative values present have no significance. Figures 6c, 7c, and 8c will depict the radial wind response [Eq. (6)], and Figs. 6d, 7d, and 8d will depict the vertical velocity response [Eq. (7)].

a. Lateral eddy heat flux convergence

The balanced response to a localized heat source is upward motion at the location of the heating, subsidence on either side, plus an inflow–outflow couplet that satisfies mass balance (e.g., Shapiro and Willoughby 1982). The resulting adiabatic warming and cooling, and tangential velocity increases and decreases, move the storm back toward balance. It is more challenging, however, to interpret the response to a field of forcing like the lateral eddy heat flux convergence [Eq. (13), term 1] shown in Fig. 6a.

Positive values represent warming by eddies. Over most of the troposphere, eddies lower the temperature. Since major hurricanes are warm-core systems (Fig. 3), eddies introduce external, relatively cooler air to the storm. Aloft, there is relatively cooler air, so eddies mix in warm air, which warms the upper troposphere and lower stratosphere.

It is the radial gradient of the heat source that drives a circulation [Eq. (8), last term]. In the lower stratosphere, the cooling by eddies is strong, but the radial gradient is small. In the 200–300-hPa layer, however, heating decreases outward between about the 600- and 800-km radii. In response, upward motion through the heating at $r = 400$ km and $p = 200$ hPa, and subsidence through the cooling outside $r = 800$ km, would be expected. Mass continuity requires outflow

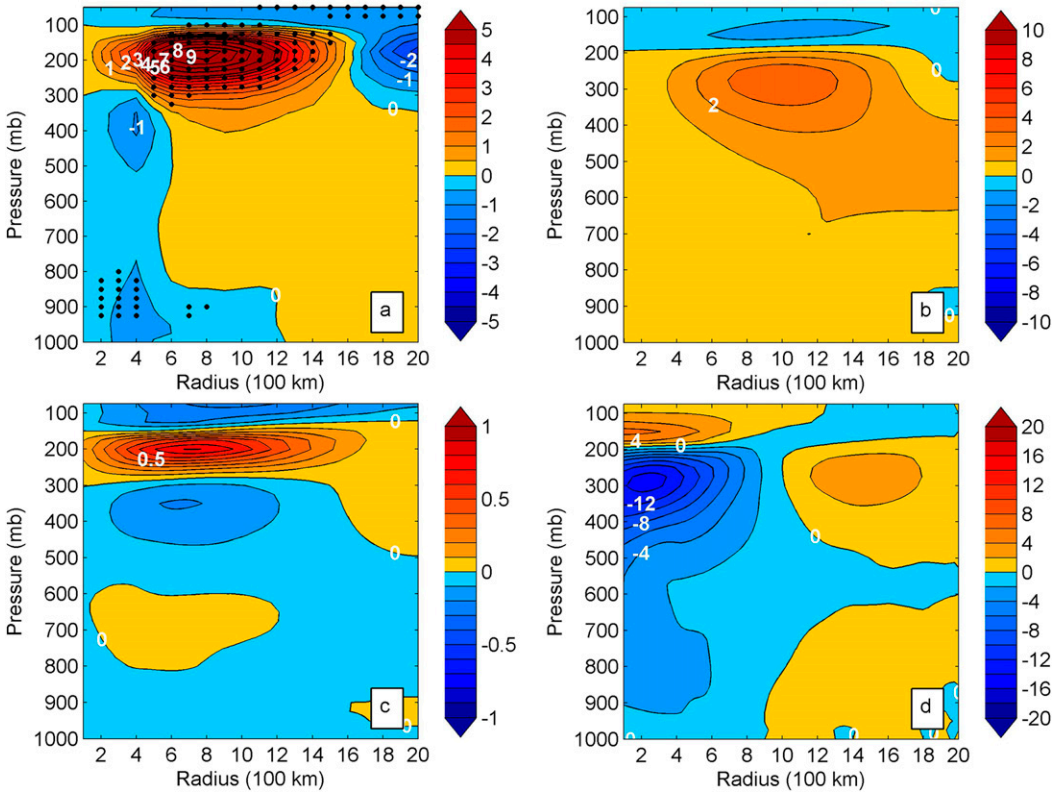

FIG. 7. As in Fig. 6, but for the lateral eddy momentum flux convergence [Eq. (14), term 1], where (a) has units of $\mathrm{m\,s^{-1}\,day^{-1}}$ and (b)–(d) have similar units as Figs. 6b–d.

above 200 hPa between the heating and cooling region and inflow below. Each of these features appears in the response to lateral eddy heat flux in Figs. 6b–d. In particular, balanced upward motion exists at upper levels in the core and weaker subsidence outside r = 800 km. Subsidence in the stratosphere at inner radii reflects the radial decrease in eddy heat fluxes near the core.

The remainder of the lateral eddy heat flux forcing is fairly weak. In the 300–400-hPa layer at large radii, cooling due to mixing with the environment increases outward (thus an outward decrease of heating), and that produces an analogous weak outflow maximum from 1800- to 2000-km radii and 300 hPa. Overall, the induced flow is weakly inward below and outward aloft, with maximum balanced vertical velocity of 6 hPa $\mathrm{day^{-1}}$ between 200 and 400 hPa at r = 400 km.

b. *Vertical eddy heat flux convergence*

The magnitude of the vertical eddy heat flux convergence [Eq. (13), term 2] is on average 0.71% of the lateral eddy heat flux convergence and lacks significant vertical and radial gradients. Therefore, the corresponding streamfunction gradients are weak, producing negligible radial wind and vertical velocity responses (not shown).

c. *Lateral eddy momentum flux convergence*

The increase in tangential velocity produced by the lateral eddy momentum flux convergence [Eq. (14), term 1] is shown in Fig. 7a. A distinct maximum exceeds 9 $\mathrm{m\,s^{-1}\,day^{-1}}$ at 175–200 hPa and r = 900 km. Figure 4b showed the maximum eddy momentum flux occurred at the 1600-km radius. Consistent with this, Fig. 7a shows flux convergence inside that radius and flux divergence outside.

As seen in Eq. (8), it is the vertical gradient of momentum forcing that drives a circulation. A local source of angular momentum produces a balanced response with outflow through the maximum source and inflow above and below. Because of the strong vertical gradients in the lateral momentum forcing, this reasoning can be applied to the field of forcing as well. The narrow induced outflow is surrounded by inflow above and below, consistent with Holland and Merrill (1984). Maximum induced outflow and upward motion from this term (Figs. 7c,d) are about 3

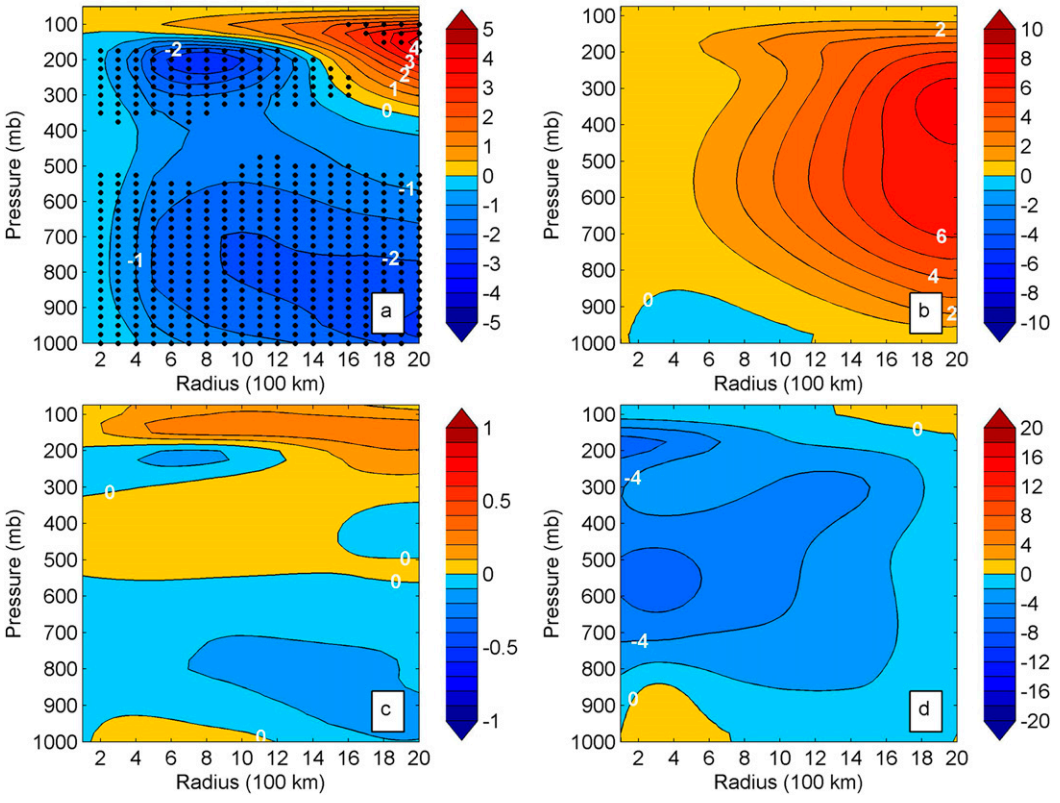

FIG. 8. As in Fig. 6, but for the eddy Coriolis torque [Eq. (14), term 3], where (a) has units of m s^{-1} day^{-1} and (b)–(d) have similar units as Figs. 6b–d.

times larger in the storm core than in the lateral eddy heat flux term (Figs. 6c,d). Subsidence in the stratosphere at small radii represents the upward decrease of momentum forcing. Subsidence occurs in the upper troposphere outside the 1600-km radius, driven by momentum flux divergence.

d. *Vertical momentum flux convergence*

Similar to the vertical eddy heat flux convergence, the vertical eddy momentum flux convergence [Eq. (14), term 2] is on average 0.38% of the lateral eddy momentum flux convergence term (not shown) and has almost no impact on the circulation.

e. *Eddy Coriolis torque*

The eddy Coriolis torque term in Eq. (14) shown in Fig. 8a was assumed to be negligible in early momentum budgets [see Table 5 from Anthes (1974)]. It is nonzero at a particular level when meridional wind averaged around the storm is nonzero. For instance, northerlies at the outer radius north of the storm have $v_r' < 0$ and $f' > 0$, making $-f'v_r' > 0$. If the same northerlies also exist to the south, then $f' < 0$ and $v_r' > 0$ in that region. The result is that azimuthal mean eddy Coriolis torque $(\overline{-f'v_r'})$ is positive. Physically, eddy inflow carries higher earth momentum from the north than eddy outflow removes from the equatorward side. This represents a momentum source at the given radius and height. The forcing is small at inner radii where f' is small. In contrast, f' at the 1500-km radius (assuming the storm lies at 20°N) is 68% larger to the north and 75% smaller to the south. In principle, the eddy Coriolis torque term can contribute to the momentum budget on those spatial scales (Frank 1977b).

The forcing associated with the eddy Coriolis torque is large and positive at outer radii from 50 to 300 hPa (Fig. 8b). The upward increase of this term in the upper troposphere drives an enhanced secondary circulation, analogous to that shown earlier for the response to lateral eddy momentum fluxes (Fig. 7b). In the storm core, the induced vertical velocity is about one-third of that from the lateral flux, but the induced upward motion fills the entire radial range (Fig. 8d).

As seen in Eq. (8), the eddy Coriolis torque drives a circulation only when it varies with height. Since f' is constant with height, the eddy Coriolis torque can drive a circulation only when mean

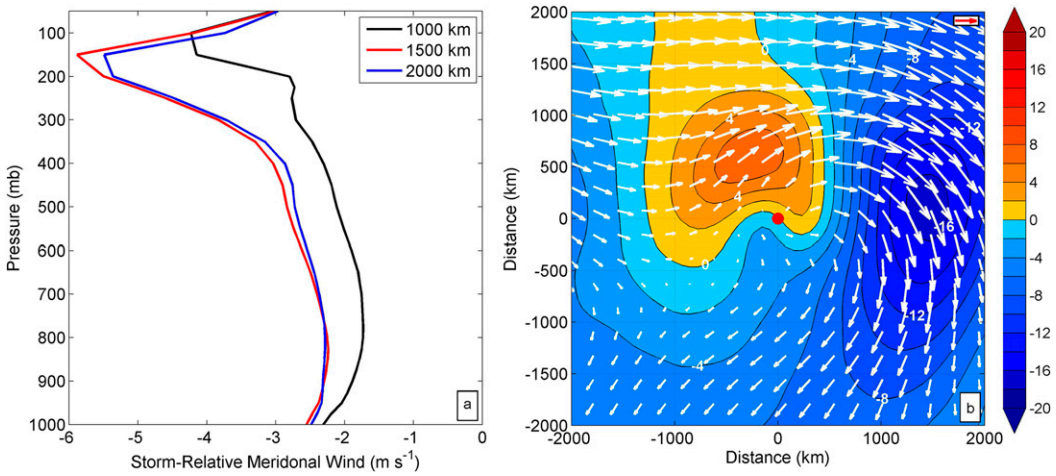

FIG. 9. (a) The vertical variation of the storm-relative meridional wind field (m s^{-1}) at three different radii: 1000 (black), 1500 (red), and 2000 km (blue). (b) Storm-centered composite of storm-relative meridional wind (shaded) and overlaying total wind (vectors) at 175 hPa for major hurricanes. Reference vector (red) is 10 m s^{-1} and the red dot at the center of the plot is the composite storm center (21.8°N, 66.2°W).

meridional wind varies with height, in particular at large radii. Figure 9a shows the mean meridional wind at three radii: 1000, 1500, and 2000 km. It is apparent that the momentum source due to flow across these radii is much stronger aloft than below, then reverses in the lower stratosphere where meridional wind decreases upward. This meridional wind reversal is consistent with the upward motion that occurs above 200 hPa in Fig. 8d.

The plan view, storm-relative composite meridional wind in the outflow layer at 175 hPa (shaded) with total wind (vectors) is shown in Fig. 9b. The reason for the negative mean meridional wind in the upper troposphere at outer radii is apparent. Strong mean northerlies occur south of the composite storm center (located at 21.8°N, 66.2°W) where outflow encounters small background inertial resistance due to smaller f near the equator. Simultaneously, mean southerlies are near zero to the north, where larger f provides larger inertial resistance. The results are the strong mean northerly winds shown in Fig. 9a.

On average, there is one anticyclonic outflow jet (vectors in Fig. 9b) that wraps around the east side of the composite storm. To the northwest of the storm center westerly flow merges with upper-level outflow, importing environmental momentum into the storm. Therefore, absolute momentum surfaces ($rv_\lambda + fr^2/2$) do not follow the prescribed in–up–out pattern as assumed by Emanuel (1986). Figure 10 shows absolute angular momentum in the major hurricanes from this study contrasted with the same field from an idealized, axisymmetric integration of the Cloud Model 1 (Bryan and Rotunno 2009).[2] In nature (Fig. 10a), outflow crosses rather than follows mean absolute momentum surfaces. These surfaces bend backward in the upper troposphere owing to the increase in tangential wind with height in Fig. 2 from 150 to 50 hPa. In contrast, the axisymmetric model (Fig. 10b) has flat absolute momentum surfaces out to the 1400-km radius in the outflow layer, thus approximating momentum conservation and indicating that air within the outflow layer is often carried from the storm center. These differences highlight the impact of eddy momentum fluxes introduced by the background environmental flow.

8. Discussion

Molinari and Vollaro (1990) first investigated the responses to eddy heat and momentum forcing in tropical cyclones in their case study of Hurricane Elena (1985). The effect of composite heat and momentum fluxes presented here is an extension of their work.

Composites of each tropical cyclone intensity group for vorticity, divergence, and the eddy heat and momentum forcing fields shown in this paper differed in their magnitude rather than their structure (Fig. 1 and

[2] Horizontal (1 km) and vertical (250 m) grid spacing were used in a 6000-km-wide and 25-km-deep domain. Thompson microphysics, NASA Goddard radiation, the Rotunno and Emanuel (1987) base-state sounding, and an SST = 28°C were employed on an f plane.

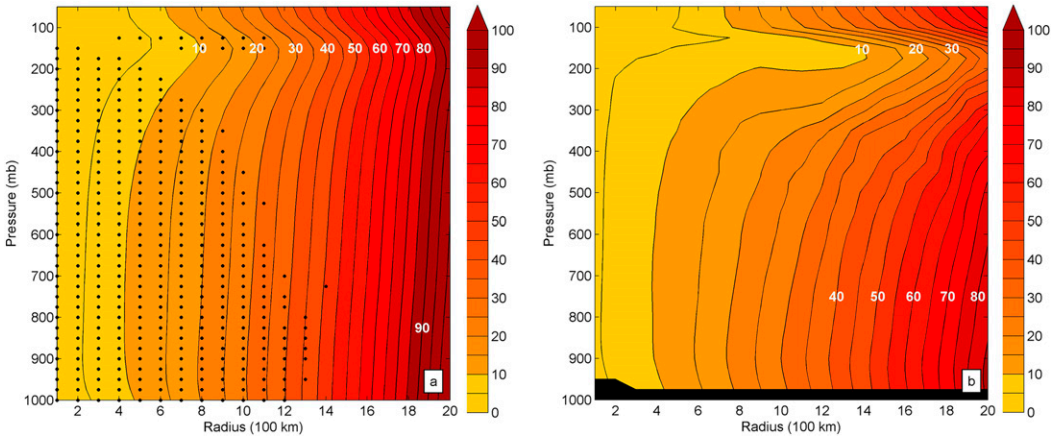

FIG. 10. The absolute angular momentum (contour interval: 5×10^6 m^2 s^{-1}) for the composite storm (a) as in Fig. 2 and (b) from CM1. Stippling (dots) in (a) indicates regions of significant differences between tropical depressions and major hurricanes as calculated by a bootstrap test. As the lowest model level in CM1 was 250 m, the conversion from height to pressure coordinates introduced missing values (black) at the bottom levels of (b).

appendix Fig. B1). As a result, only major hurricanes were shown, along with the regions where they differed significantly from tropical depressions. Both inflow and outflow extended from the center to beyond the 2000-km radius. Outflow reached a maximum in a narrow layer (100–300 hPa) centered at $p = 175$ hPa and $r = 600$ km (Fig. 2a). Anticyclonic flow peaked in the outflow layer at $p = 175$ hPa and $r = 1200$ km (Fig. 2b). Inflow and cyclonic tangential velocity were largest near the surface at inner radii. Surface tangential velocity remained cyclonic out to the 1400-km radius. These fields were broadly similar to the composites of Frank (1977a) and Holland and Merrill (1984) using rawinsonde data.

The extended inflow and outflow layers have several implications for the budget of angular momentum. Smith et al. (2014) argued that at large radii, the mean flux of angular momentum in isolated tropical cyclones on an f plane must be negligible. While this might hold for isolated disturbances, it clearly is not the case in storms in nature. The extended outflow layer insures that even at large radii the mean angular momentum flux (Fig. 4a) was an appreciable fraction of the eddy flux.

Figure 2b showed that anticyclonic flow reached the surface outside the 1400-km radius. Within that radius, horizontal eddy momentum fluxes provided the only source of momentum to balance friction, as noted by Anthes (1974). Outside 1400 km, consistent with the comments of Smith et al. (2014), both the frictional gain of momentum in the surface anticyclonic flow and the lateral eddy fluxes contributed cyclonic momentum to offset the loss to friction.

The Eliassen (1952) balanced vortex equation was solved for all eddy heat and momentum forcing terms. Even though the heat and momentum forcings were largest in the upper troposphere (Figs. 6a, 7a, 8a), the response was felt through the entire depth of the troposphere owing to low static stability beneath the forcing. The lateral momentum flux produced the largest response, with induced vertical velocity in the core more than twice as large as the lateral eddy heat flux and eddy Coriolis torque. Lateral eddy heat flux convergence was large, but its radial gradient was generally small, making for a smaller response. Overall, the eddy momentum source terms generated a greater response than the eddy heat source terms.

The eddy Coriolis torque was the most intriguing term. Smith et al. (2014) state that nowhere does the planetary angular momentum enter the angular momentum balance for isolated vortices on an f plane. The results of this paper show that such an assumption cannot be made in storms in nature. The mean Coriolis torque nearly vanished, but eddy Coriolis torque arose as a result of a negative mean meridional velocity at outer radii in the upper troposphere. This circulation created larger eddy inflow of Earth momentum to the north than it removed to the south. The eddy Coriolis torque drove a deep circulation because the forcing term varied with height. The result was broad upward motion at all radii that peaked in the storm core. Mean wind maps indicated that the eddy Coriolis torque was driven by background variations in inertial stability between low and high latitudes. This source term is another outcome of the extended outflow layer. Such differences between isolated idealized storms and storms in nature provide challenges to bridging the gap between theory and observations.

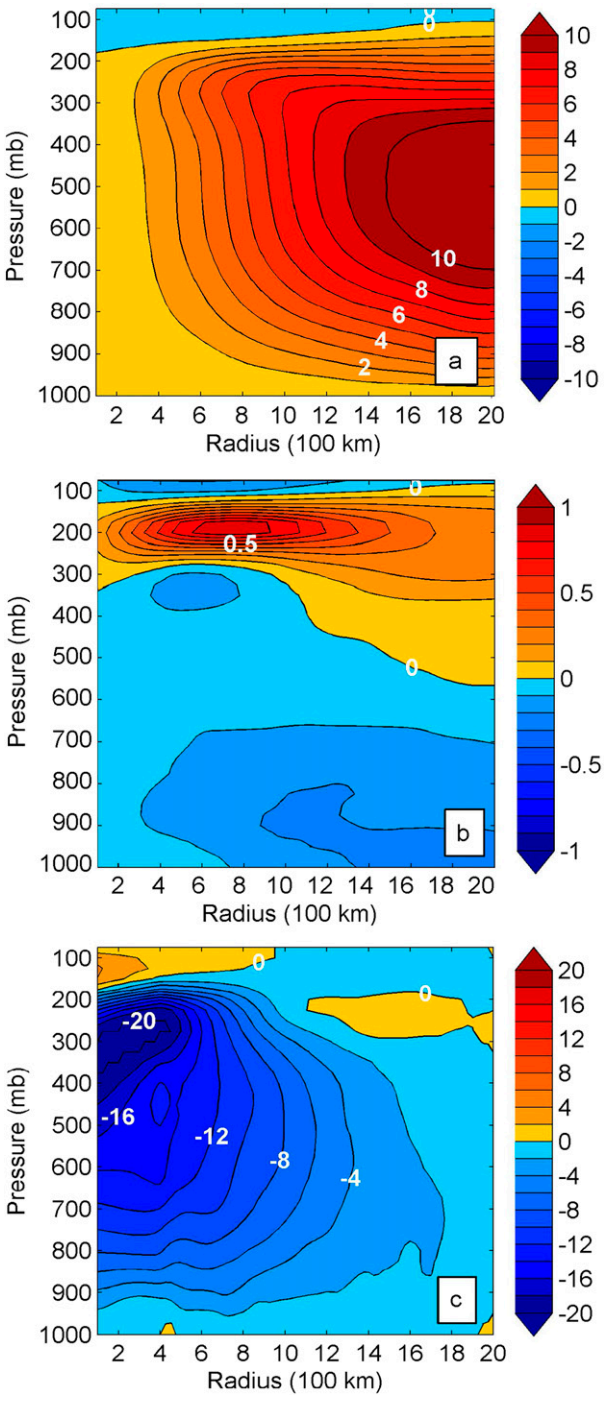

FIG. 11. The vortex response with all forcing terms included for the (a) streamfunction (contour interval: 1×10^9 Pa m^2 s^{-1}), (b) radial wind (contour interval: 0.1 m s^{-1}), and (c) vertical velocity (2 hPa day^{-1}).

Figure 11 depicts the streamfunction and associated radial and vertical velocity for the sum of all eddy terms. Taken together, eddy fluxes aloft at outer radii drive radial–vertical motions throughout the depth of the troposphere at all radii, including at inner radii. There is inflow in the lower troposphere, outflow aloft, and a broad upward motion that peaks in the upper troposphere at small radii. It is thus apparent that eddy forcing contributes positively to tropical cyclone radial–vertical circulation. Additionally, the upper-tropospheric peak of vertical motion could aid in destabilization and thus couple with more intense convection. Inflow at outer radii could be indicative of storm expansion (Merrill 1984) and the increased inflow above the boundary layer at smaller radii could contribute to the spinup of the primary circulation (Ooyama 1969).

The challenge is to evaluate quantitatively the role of this forcing in tropical cyclones. Pfeffer and Challa (1981) assessed the impact of lateral eddy momentum fluxes by simply inserting them into an axisymmetric model. It is proposed that the same can be done with the terms in this study, both individually and combined, and for various intensity ranges, to evaluate their role in tropical cyclone formation and intensification.

Acknowledgments. SDD conducted research with Government support under and awarded by DoD, Air Force Office of Scientific Research, National Defense Science and Engineering Graduate (NDSEG) Fellowship, 32 CFR 168a. JM and DV were supported by Office of Naval Research Grant N000141410162. The ERA-Interim data used for this research were retrieved from the Research Data Archive (RDA), which is maintained by the Computational and Information Systems Laboratory (CISL) at the National Center for Atmospheric Research (NCAR). The original data are available from the RDA (http://rda.ucar.edu/datasets/ds627.0/).

APPENDIX A

The Impacts of the Global Analyses Resolution

a. Differences in storm center positions

Storm center positions in ERA-Interim often differ from best track estimates from HURDAT2. Likely as a result of this, unrealistic lateral eddy momentum flux convergence was present at inner radii (Fig. A1b). Values near the surface reached -8 m s^{-1} day^{-1} and decreased in magnitude with height. In response, the balanced vertical velocity showed upward motion directly in the core where momentum flux increased upward (Fig. A2b). Other dominant forcing field terms did not show unrealistic values at inner radii (Figs. A1a,c). To remove the lateral eddy

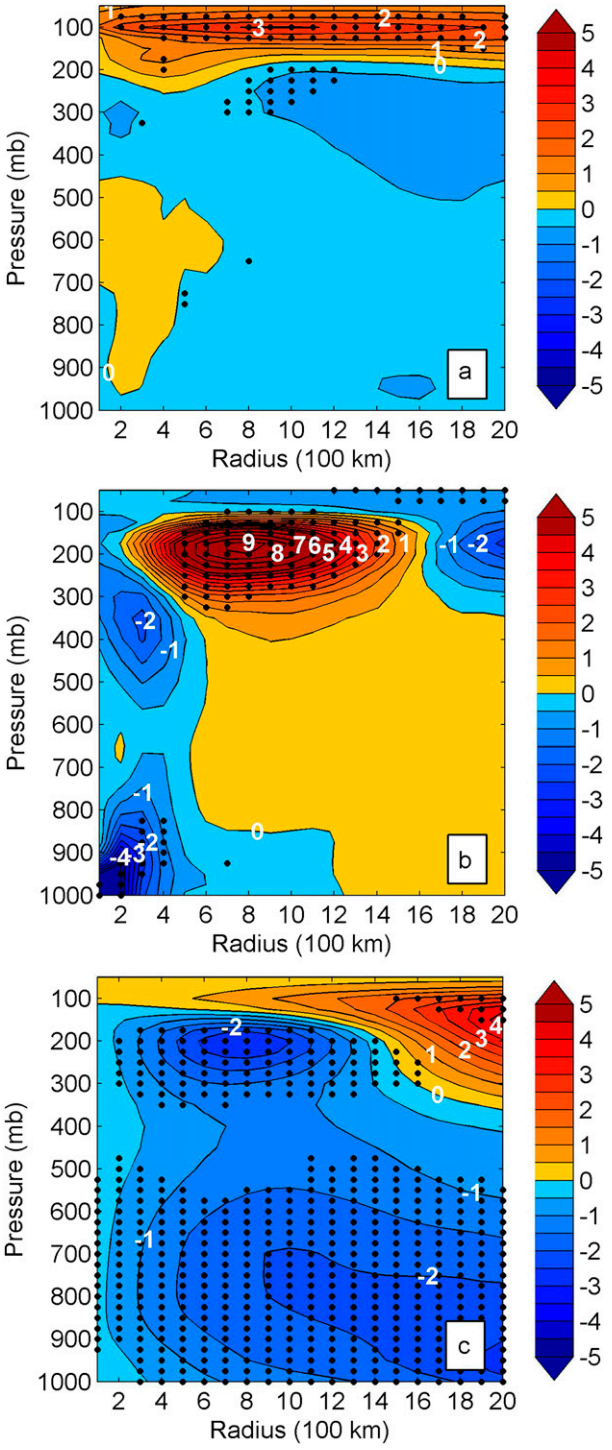

FIG. A1. The nonsmoothed dominant forcing terms for major hurricanes: (a) the lateral eddy heat flux convergence [Eq. (13), term 1] composite (compare to Fig. 6a), (b) the lateral eddy momentum flux convergence [Eq. (14), term 1] composite (compare to Fig. 7a), and (c) the eddy Coriolis torque [Eq. (14), term 3] composite (compare to Fig. 8a). Stippling (dots) indicates regions of significant differences between tropical depressions and major hurricanes as calculated by a bootstrap test.

momentum flux convergence artifact, all forcing terms in Eqs. (13) and (14) were linearly interpolated from their values at the 400-km radius to zero at the center. This procedure minimized the influence of differences in storm center position between the ERA-Interim and the best track center positions used to define the cylindrical grids. This appendix will show that the procedures we used had little impact on the results, except to remove one unphysical result.

Figure A2 shows the nonsmoothed (Figs. A2a–c) and smoothed (Figs. A2d–f) vertical velocity responses for the three dominant eddy heat and momentum source terms. Figures A2d–f are analogous to Figs. 6d, 7d, and 8d, respectively. The largest difference between the nonsmoothed and smoothed vertical velocity responses is present in the lateral eddy momentum flux convergence term within the inner core in the boundary layer (Fig. A2b). Wind gradients in nature are enormous at inner radii and thus the effects of center position differences would be expected to be largest there. The smoothing removed the unphysical lower-tropospheric upward motion due to lateral momentum fluxes in the storm core. More importantly, the remainder of the solution at all radii and heights were virtually unchanged, as seen when comparing all other points in Figs. A2b–e. The other two dominant forcing terms shown contain much smaller differences than the lateral eddy momentum flux convergence and similar responses with and without interpolation of the forcing.

With the exception of the lower-tropospheric upward motion in Fig. A2b, center position differences between ERA-Interim and HURDAT2 have a negligible impact on the balanced solutions. This lack of influence arises because of the small area represented by the storm core and the smoothing effect of the inverse Laplacian.

b. *Applying major hurricane eddy forcings on the tropical depression mean field*

ERA-Interim underestimates radial velocity, and thus the mean fields in the storm core are not fully represented. This appendix will show that underestimating the basic state at inner radii does not affect the outcome of the balanced vortex equation.

The response to the eddy forcing from major hurricanes is calculated using the mean fields from tropical depressions. The maximum tangential wind speed of tropical depressions is four times smaller than that in major hurricanes, and thus tropical depressions have a much smaller inertial stability. In addition, the tropical depression potential temperature anomaly is 4.5 K smaller than that in major hurricanes.

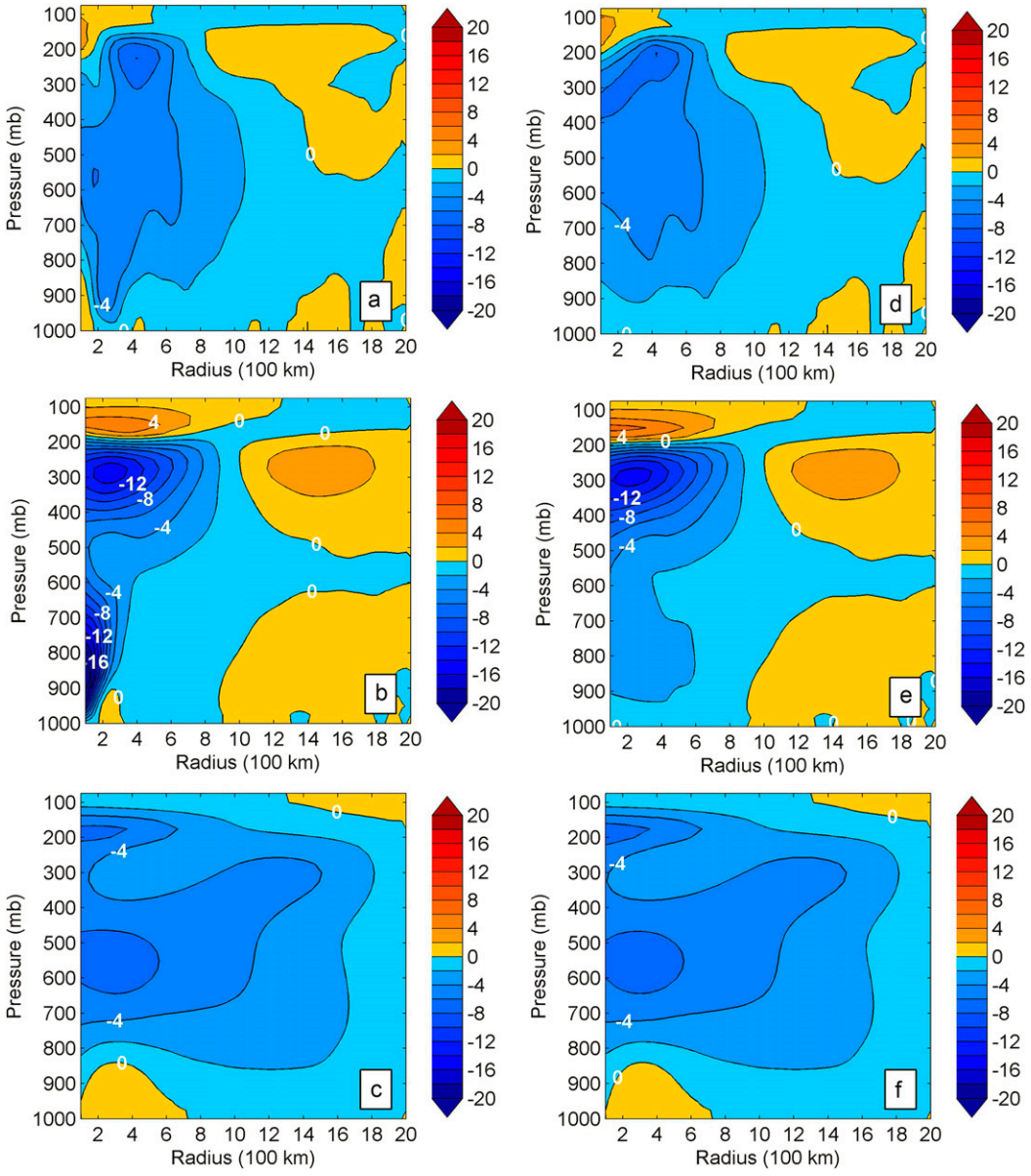

FIG. A2. Comparison of the vertical velocity response to the (a)–(c) nonsmoothed and (d)–(f) smoothed eddy fluxes (contour interval: 2 hPa day^{-1}) for (a),(d) lateral eddy heat flux convergence; (b),(e) lateral eddy momentum flux convergence; and (c),(f) eddy Coriolis torque.

Fig. A3 depicts the radial and vertical velocity response for the sum of all eddy terms, analogous to Figs. 11b and 11c, respectively. The vertical velocity responses are remarkably similar despite the significantly different mean state. This implies that 1) the inverse Laplacian operator smooths out the influence of basic-state differences in the physically small core region and 2) the eddy forcing is mostly on larger scales outside the core. Thus, even though ERA-Interim underestimates the magnitude of the radial and tangential wind fields of tropical cyclones and the inertial stability in the inner core, this underestimation does not affect the balanced model calculations.

APPENDIX B

Variation of Eddy Forcing with Intensity

This appendix will show how forcing terms are remarkably similar structurally regardless of intensity.

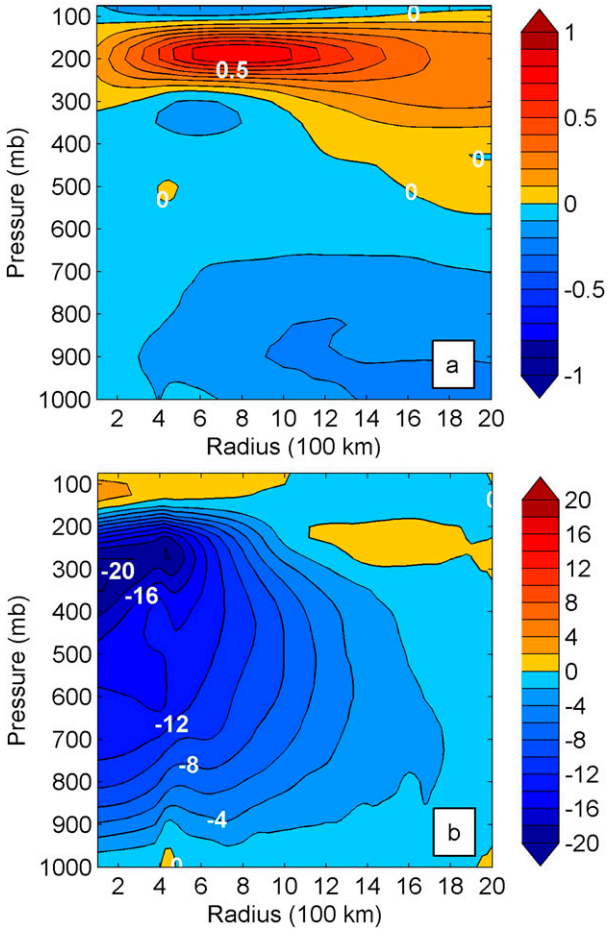

FIG. A3. (a) The radial wind (contour interval: 0.1 m s^{-1}) and (b) the vertical velocity (2 hPa day^{-1}) responses of the tropical depression mean vortex to major hurricane eddy forcings with all forcing terms included.

The composite forcing fields for tropical depressions for the three dominant eddy heat and momentum source terms (the lateral eddy heat flux convergence, the lateral eddy momentum flux convergence, and the eddy Coriolis torque) are shown in Fig. B1. They are analogous to Figs. 6a, 7a, and 8a, respectively. Note how structurally, all forcing fields are very similar. Differences manifest primarily in the magnitude of the forcing field. For that reason, only the major hurricane responses are detailed in the text.

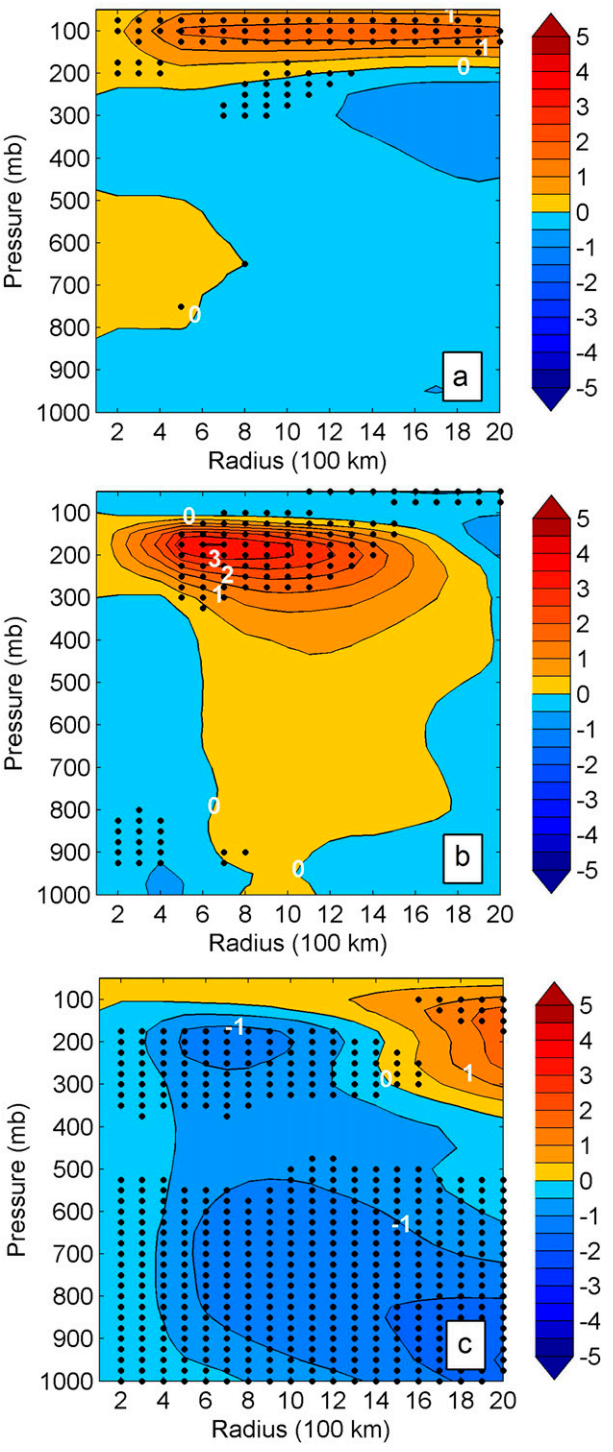

FIG. B1. Dominant forcing terms for tropical depressions: (a) the lateral eddy heat flux convergence [Eq. (13), term 1] composite (compare to Fig. 6a), (b) the lateral eddy momentum flux convergence [Eq. (14), term 1] composite (compare to Fig. 7a), and (c) the eddy Coriolis torque [Eq. (14), term 3] composite (compare to Fig. 8a). Stippling (dots) indicates regions of significant differences between tropical depressions and major hurricanes as calculated by a bootstrap test.

REFERENCES

Anthes, R. A., 1974: The dynamics and energetics of mature tropical cyclones. *Rev. Geophys. Space Phys.*, **12**, 495–522, doi:10.1029/RG012i003p00495.

Bryan, G. H., and R. Rotunno, 2009: The maximum intensity of tropical cyclones in axisymmetric numerical model simulations. *Mon. Wea. Rev.*, **137**, 1770–1789, doi:10.1175/2008MWR2709.1.

Dee, D. P., and Coauthors, 2011: The ERA-Interim reanalysis: Configuration and performance of the data assimilation system. *Quart. J. Roy. Meteor. Soc.*, **137**, 553–597, doi:10.1002/qj.828.

DeMaria, M., and J. Kaplan, 1994: A Statistical Hurricane Intensity Prediction Scheme (SHIPS) for the Atlantic basin. *Wea. Forecasting*, **9**, 209–220, doi:10.1175/1520-0434(1994)009<0209:ASHIPS>2.0.CO;2.

Dunion, J. P., 2011: Rewriting the climatology of the tropical North Atlantic and Caribbean Sea atmosphere. *J. Climate*, **24**, 893–908, doi:10.1175/2010JCLI3496.1.

Eliassen, A., 1952: Slow thermally or frictionally controlled meridional circulation in a circular vortex. *Astrophys. Norv.*, **5**, 19–60.

Emanuel, K. A., 1986: An air-sea interaction theory for tropical cyclones. Part I: Steady-state maintenance. *J. Atmos. Sci.*, **43**, 585–605, doi:10.1175/1520-0469(1986)043<0585:AASITF>2.0.CO;2.

——, and R. Rotunno, 2011: Self-stratification of tropical cyclone outflow. Part I: Implications for storm structure. *J. Atmos. Sci.*, **68**, 2236–2249, doi:10.1175/JAS-D-10-05024.1.

Frank, W. M., 1977a: The structure and energetics of the tropical cyclone I. Storm structure. *Mon. Wea. Rev.*, **105**, 1119–1135, doi:10.1175/1520-0493(1977)105<1119:TSAEOT>2.0.CO;2.

——, 1977b: The structure and energetics of the tropical cyclone II. Dynamics and energetics. *Mon. Wea. Rev.*, **105**, 1136–1150, doi:10.1175/1520-0493(1977)105<1136:TSAEOT>2.0.CO;2.

Holland, G. J., and R. T. Merrill, 1984: On the dynamics of tropical cyclone structural changes. *Quart. J. Roy. Meteor. Soc.*, **110**, 723–745, doi:10.1002/qj.49711046510.

Landsea, C. W., and J. L. Franklin, 2013: Atlantic hurricane database uncertainty and presentation of a new database format. *Mon. Wea. Rev.*, **141**, 3576–3592, doi:10.1175/MWR-D-12-00254.1.

McBride, J. L., 1981: Observational analysis of tropical cyclone formation. Part I: Basic description of data sets. *J. Atmos. Sci.*, **38**, 1117–1131, doi:10.1175/1520-0469(1981)038<1117:OAOTCF>2.0.CO;2.

Merrill, R. T., 1984: A comparison of large and small tropical cyclones. *Mon. Wea. Rev.*, **112**, 1408–1418, doi:10.1175/1520-0493(1984)112<1408:ACOLAS>2.0.CO;2.

Molinari, J., and D. Vollaro, 1989: External influences on hurricane intensity. Part I: Outflow layer eddy angular momentum fluxes. *J. Atmos. Sci.*, **46**, 1093–1105, doi:10.1175/1520-0469(1989)046<1093:EIOHIP>2.0.CO;2.

——, and ——, 1990: External influences on hurricane intensity. Part II: Vertical structure and response of the hurricane vortex. *J. Atmos. Sci.*, **47**, 1902–1918, doi:10.1175/1520-0469(1990)047<1902:EIOHIP>2.0.CO;2.

Ooyama, K., 1969: Numerical simulation of the life cycle of tropical cyclones. *J. Atmos. Sci.*, **26**, 3–40, doi:10.1175/1520-0469(1969)026<0003:NSOTLC>2.0.CO;2.

Pfeffer, R. L., and M. Challa, 1981: A numerical study of the role of eddy fluxes of momentum in the development of Atlantic hurricanes. *J. Atmos. Sci.*, **38**, 2393–2398, doi:10.1175/1520-0469(1981)038<2393:ANSOTR>2.0.CO;2.

Rappin, E. D., M. C. Morgan, and G. J. Tripoli, 2011: The impact of outflow environment on tropical cyclone intensification and structure. *J. Atmos. Sci.*, **68**, 177–194, doi:10.1175/2009JAS2970.1.

Rotunno, R., and K. A. Emanuel, 1987: An air–sea interaction theory for tropical cyclones. Part II: Evolutionary study using a nonhydrostatic axisymmetric numerical model. *J. Atmos. Sci.*, **44**, 542–561, doi:10.1175/1520-0469(1987)044<0542:AAITFT>2.0.CO;2.

Schenkel, B. A., and R. E. Hart, 2012: An examination of tropical cyclone position, intensity, and intensity life cycle within atmospheric reanalysis datasets. *J. Climate*, **25**, 3453–3475, doi:10.1175/2011JCLI4208.1.

Shapiro, L. J., and H. E. Willoughby, 1982: The response of balanced hurricanes to local sources of heat and momentum. *J. Atmos. Sci.*, **39**, 378–394, doi:10.1175/1520-0469(1982)039<0378:TROBHT>2.0.CO;2.

Simpson, R. H., 1974: The hurricane disaster potential scale. *Weatherwise*, **27**, 169–186, doi:10.1080/00431672.1974.9931702.

Smith, R. K., M. T. Montgomery, and J. Persing, 2014: On steady-state tropical cyclones. *Quart. J. Roy. Meteor. Soc.*, **140**, 2638–2649, doi:10.1002/qj.2329.

Stern, D. P., and D. S. Nolan, 2012: On the height of the warm core in tropical cyclones. *J. Atmos. Sci.*, **69**, 1657–1680, doi:10.1175/JAS-D-11-010.1.

Torn, R. D., and C. Snyder, 2012: Uncertainty of tropical cyclone best-track information. *Wea. Forecasting*, **27**, 715–729, doi:10.1175/WAF-D-11-00085.1.